Research Article | Vol. 9, No. 6 | 1 Jun 2018 | BIOMEDICAL OPTICS EXPRESS 2575
Biomedical Optics EXPRESS

Computational analysis of linear energy modulation for laser thermal coagulation

VAN NAM TRAN,[1] VAN GIA TRUONG,[1] SEOK JEONG,[2] AND HYUN WOOK KANG[3,*]

[1]*Interdisciplinary Program of Marine-Bio, Electrical & Mechanical Engineering, Pukyong National University, Busan, South Korea*
[2]*Division of Gastroenterology, Department of Internal Medicine, Inha University Hospital, Incheon, South Korea*
[3]*Department of Biomedical Engineering and Center for Marine-Integrated Biomedical Technology (BK21 Plus), Pukyong National University, Busan, South Korea*
**wkang@pukyong.ac.kr*

Abstract: Accurate treatment planning and monitoring are critical factors to ensure safe and effective outcomes of laser thermal coagulation (LTC). Computational and experimental models based upon linear energy modulation were deployed to predict temperature distribution and thermal damage within *ex vivo* porcine liver. 1470-nm Gaussian emission was confirmed by using digital imaging and the customized goniometry. The tissue temperature was maintained in the pre-determined range (65~75 °C) to induce thermally destructive volumes of 0.23 cm^3 (simulation) and 0.17 ± 0.05 cm^3 (experiment) once the applied power was linearly reduced from 3.5 W to 0.2 W in 50 s ("3.5 W fast slope" laser modulation mode). The proposed model may be a useful tool to predict thermal responses of the tissue during LTC.

OCIS codes: (060.2280) Fiber design and fabrication; (140.3510) Lasers, fiber; (170.1020) Ablation of tissue; (170.3660) Light propagation in tissues; (170.6935) Tissue characterization.

References and links

1. R. Medvid, A. Ruiz, R. J. Komotar, J. R. Jagid, M. E. Ivan, R. M. Quencer, and M. B. Desai, "Current applications of MRI-guided laser interstitial thermal therapy in the treatment of brain neoplasms and epilepsy: a radiologic and neurosurgical overview," AJNR Am. J. Neuroradiol. **36**(11), 1998–2006 (2015).
2. M. J. LaRiviere and R. E. Gross, "Stereotactic laser ablation for medically intractable epilepsy: the next generation of minimally invasive epilepsy surgery," Front. Surg. **3**, 64 (2016).
3. A. Carpentier, R. J. McNichols, R. J. Stafford, J. P. Guichard, D. Reizine, S. Delaloge, E. Vicaut, D. Payen, A. Gowda, and B. George, "Laser thermal therapy: real-time MRI-guided and computer-controlled procedures for metastatic brain tumors," Lasers Surg. Med. **43**(10), 943–950 (2011).
4. A. Carpentier, R. J. McNichols, R. J. Stafford, J. Itzcovitz, J.-P. Guichard, D. Reizine, S. Delaloge, E. Vicaut, D. Payen, A. Gowda, and B. George, "Real-time magnetic resonance-guided laser thermal therapy for focal metastatic brain tumors," Neurosurgery **63**(1), ONS21–ONS28, discussion ONS28–ONS29 (2008).
5. S. van Esser, G. Stapper, P. J. van Diest, M. A. van den Bosch, J. H. Klaessens, W. P. Mali, I. H. Borel Rinkes, and R. van Hillegersberg, "Ultrasound-guided laser-induced thermal therapy for small palpable invasive breast carcinomas: a feasibility study," Ann. Surg. Oncol. **16**(8), 2259–2263 (2009).
6. Y. Kerbage, N. Betrouni, P. Collinet, H. Azaïs, S. Mordon, A.-S. Dewalle-Vignion, and B. Merlot, "Laser interstitial thermotherapy application for breast surgery: Current situation and new trends," Breast **33**, 145–152 (2017).
7. A. Masters, A. C. Steger, W. R. Lees, K. M. Walmsley, and S. G. Bown, "Interstitial laser hyperthermia: a new approach for treating liver metastases," Br. J. Cancer **66**(3), 518–522 (1992).
8. M. G. Skinner, M. N. Iizuka, M. C. Kolios, and M. D. Sherar, "A theoretical comparison of energy sources--microwave, ultrasound and laser--for interstitial thermal therapy," Phys. Med. Biol. **43**(12), 3535–3547 (1998).
9. D. I. Fielding, G. Buonaccorsi, A. Hanby, M. R. Hetzel, and S. G. Bown, "Interstitial laser photocoagulation of normal lung parenchyma in rats," Thorax **53**(8), 692–697 (1998).
10. T. A. McNicholas, A. C. Steger, and S. G. Bown, "Interstitial Laser Coagulation of the Prostate. An Experimental Study," Br. J. Urol. **71**(4), 439–444 (1993).
11. E. Schena, P. Saccomandi, and Y. Fong, "Laser ablation for cancer: past, present and future," J. Funct. Biomater. **8**(2), 19 (2017).

#324526 https://doi.org/10.1364/BOE.9.002575
Journal © 2018 Received 20 Feb 2018; revised 5 Apr 2018; accepted 1 May 2018; published 9 May 2018

Biomedical Optics EXPRESS

12. A. Welch, "The thermal response of laser irradiated tissue," IEEE J. Quantum Electron. **20**(12), 1471–1481 (1984).
13. S. Thomsen, "Pathologic analysis of photothermal and photomechanical effects of laser-tissue interactions," Photochem. Photobiol. **53**(6), 825–835 (1991).
14. G. K. Eyrich, E. Bruder, P. Hilfiker, B. Dubno, H. H. Quick, M. A. Patak, K. W. Grätz, and H. F. Sailer, "Temperature mapping of magnetic resonance-guided laser interstitial thermal therapy (LITT) in lymphangiomas of the head and neck," Lasers Surg. Med. **26**(5), 467–476 (2000).
15. C. Hoppe, J.-A. Witt, C. Helmstaedter, T. Gasser, H. Vatter, and C. E. Elger, "Laser interstitial thermotherapy (LiTT) in epilepsy surgery," Seizure **48**, 45–52 (2017).
16. I. Mellal, A. Oukaira, E. Kengene, and A. Lakhssassi, "Thermal Therapy Modalities for Cancer Treatment: A Review and Future Perspectives," Appl. Sci. Res. Rev. **4**, 14 (2017).
17. G. J. Müller and A. Roggan, *Laser-induced Interstitial Thermotherapy* (SPIE Press, 1995).
18. V. X. Du, S. V. Gandhi, H. L. Rekate, and A. D. Mehta, "Laser interstitial thermal therapy: A first line treatment for seizures due to hypothalamic hamartoma?" Epilepsia **58**(S2), 77–84 (2017).
19. T. H. Nguyen, S. Park, K. K. Hlaing, and H. W. Kang, "Temperature feedback-controlled photothermal treatment with diffusing applicator: theoretical and experimental evaluations," Biomed. Opt. Express **7**(5), 1932–1947 (2016).
20. D. Tosi, E. G. Macchi, G. Braschi, A. Cigada, M. Gallati, S. Rossi, S. Poeggel, G. Leen, and E. Lewis, "Fiber-optic combined FPI/FBG sensors for monitoring of radiofrequency thermal ablation of liver tumors: ex vivo experiments," Appl. Opt. **53**(10), 2136–2144 (2014).
21. G. Palumbo, D. Tosi, E. Schena, C. Massaroni, J. Ippolito, P. Verze, N. Carlomagno, V. Tammaro, A. Iadicicco, and S. Campopiano, "Real-time temperature monitoring during radiofrequency treatments on ex-vivo animal model by fiber Bragg grating sensors," in *Optical Sensors 2017* (International Society for Optics and Photonics, 2017), 102312K.
22. N. T. Pham, S. L. Lee, S. Park, Y. W. Lee, and H. W. Kang, "Real-time temperature monitoring with fiber Bragg grating sensor during diffuser-assisted laser-induced interstitial thermotherapy," J. Biomed. Opt. **22**(4), 045008 (2017).
23. P. Saccomandi, E. Schena, and S. Silvestri, "Techniques for temperature monitoring during laser-induced thermotherapy: an overview," Int. J. Hyperthermia **29**(7), 609–619 (2013).
24. E. Schena, D. Tosi, P. Saccomandi, E. Lewis, and T. Kim, "Fiber optic sensors for temperature monitoring during Thermal Treatments: An overview," Sensors (Basel) **16**(7), 1144 (2016).
25. J. D. Voigt and G. Barnett, "The value of using a brain laser interstitial thermal therapy (LITT) system in patients presenting with high grade gliomas where maximal safe resection may not be feasible," Cost Eff. Resour. Alloc. **14**(1), 6 (2016).
26. V. N. Tran, H. Lee, V. G. Truong, Y. Rhee, and H. W. Kang, "Concentric photothermal coagulation with basket-integrated optical device for treatment of tracheal stenosis," J. Biophotonics **11**(1), e201700073 (2017).
27. R. Steiner, "Laser-tissue interactions," in *Laser and IPL Technology in Dermatology and Aesthetic Medicine* (Springer, 2011), pp. 23–36.
28. J. Kwon, C.-Y. Lee, J. Oh, and H. W. Kang, "Computational analysis of endometrial photocoagulation with diffusing optical device," Biomed. Opt. Express **4**(11), 2450–2462 (2013).
29. S. R. Mordon, B. Wassmer, and J. Zemmouri, "Mathematical modeling of endovenous laser treatment (ELT)," Biomed. Eng. Online **5**(1), 26 (2006).
30. J. P. Ritz, A. Roggan, C. Isbert, G. Müller, H. J. Buhr, and C. T. Germer, "Optical properties of native and coagulated porcine liver tissue between 400 and 2400 nm," Lasers Surg. Med. **29**(3), 205–212 (2001).
31. D. Salvi, D. Boldor, J. Ortego, G. M. Aita, and C. M. Sabliov, "Numerical modeling of continuous flow microwave heating: a critical comparison of COMSOL and ANSYS," J. Microw. Power Electromagn. Energy **44**(4), 187–197 (2010).
32. P. Tombesi, F. Di Vece, and S. Sartori, "Radiofrequency, microwave, and laser ablation of liver tumors: time to move toward a tailored ablation technique," Hepatoma Res. **1**(2), 52–57 (2015).
33. F. M. Di Matteo, P. Saccomandi, M. Martino, M. Pandolfi, M. Pizzicannella, V. Balassone, E. Schena, C. M. Pacella, S. Silvestri, and G. Costamagna, "Feasibility of EUS-guided Nd:YAG laser ablation of unresectable pancreatic adenocarcinoma," Gastrointest. Endosc. S0016-5107(18)30110-X (2018).

1. Introduction

Laser thermal coagulation (LTC) has been considered a minimally invasive treatment for stereotactic tumors. LTC uses heat from optical fibers to disrupt neoplastic tissue based upon thermal coagulation and necrosis. LTC has recently been applied for treatment of epilepsy [1, 2] and tumors in brain [3, 4], breast [5, 6], liver [7, 8], lung [9], prostate [10], and pancreas [11]. In spite of various types of surgical fibers, treatment outcomes are dependent not only on tissue properties but also on treatment parameters such as irradiation time, power, and spot size [12]. As a result, the resultant thermal effects may occur differently within the tissue due to spatial and temporal distribution of temperature. Protein denaturation, hyalinization of

Biomedical Optics EXPRESS

collagen, and cell shrinkage may take place once the tissue temperature exceeds 60~65°C (threshold of tissue coagulation). As the temperature increases more than 300°C, carbonization and tissue ablation may be observed [13–15].

The main advantages of LTC technique include minimal invasiveness, high precision, less pain, and faster recovery, compared with traditional open surgical methods [16]. However, LTC still suffers from high temperature at the fiber tip, non-uniform lesion through the treated volume, inaccurate placement of the laser fiber into the target lesion, and especially difficulty in managing the thermal necrosis region to match with the target shape due to the lack of real-time control and treatment planning system [6, 11, 17]. To attain deep tissue denaturation, LTC is usually deployed for various times (30 s ~10 min), depending on various diseases [1, 3, 14, 18]. However, surface shrinkage and/or carbonization may be observed due to substantial thermal development. In addition, the overheated irradiation on the target region may affect adjacent healthy tissues, leading to many undesirable post-operative side-effects such as delayed healing response [19].

Therefore, planning and monitoring techniques have been increasingly proposed to predict and manage the temperature development and thermal coagulated volumes during the treatment. These techniques may be divided into two groups: invasiveness including thermistor, and thermocouple, fiber optic sensors [19–22], and non-invasiveness including magnetic resonance imaging (MRI), computed topography (CT), and ultrasound (US)-based thermometry [8, 23, 24]. However, thermocouples may absorb the light due to their metallic materials while fiber optic sensors are expensive and sensitive to the tissue strain (i.e., movement of organs due to respiration), leading to overestimation during the measurement. By contrast, thermography techniques based on CT, US, and MRI lack real-time and accurate feedback. Moreover, these techniques are more complicated and expensive than the invasiveness groups [15, 16, 24, 25]. Interestingly, although the temperature feedback issue within the tissue might be pivotal to help surgeons adjust laser settings, LTC is usually performed without the real-time monitoring of tissue temperature [23]. Thus, further models should be developed to support and simplify the screening step of the LTC procedure, eventually enhancing therapeutic outcomes. Therefore, the main goal of the current study is to evaluate the feasibility of linear energy modulation in computational and experimental models for effective LTC on small-sized tumors. It was hypothesized that application of the linear energy modulation could achieve the steady tissue temperature and predict the distribution of thermal lesion in a pre-determined manner.

2. Materials and methods

2.1. Physical model for simulation

A 3D geometry used for the current simulation model consisted of two parts: liver tissue and flat optical fiber. The tissue was constructed in a cubic shape with physical dimensions of 5 cm × 5 cm × 3 cm (i.e., volume = 75 cm^3). The flat fiber was 400 μm in core diameter and its numerical aperture (NA) was 0.22. The fiber tip was vertically situated 2.6 cm above the tissue surface, and the corresponding beam spot size on the tissue surface was 1.2 cm in diameter. The liver tissue was assumed to be homogenous and isotropic.

2.2. Fiber preparation

A multimode 400-μm core diameter flat fiber (FIP400440480; Molex Inc., Lisle, Illinois, USA) was used in this study. To evaluate the fiber performance, a customized goniometer in conjunction with a photodiode (PD-300-3W; Ophir, Jerusalem, Israel) was deployed to measure the spatial light distribution from the fiber. A 632-nm light from HeNe laser source was selected for the emission measurements due to its visual observations. The photodiode was controlled by using LabView software to circle around the center position of the fiber tip with a radius of 2.6 cm at the speed of 0.05 rad/s. The measured intensities were then

Biomedical Optics EXPRESS

normalized to minimize any effect of laser power fluctuations on the measurements. To validate the acquired goniometric results, a camera (Canon-70D-18-55, Canon Park, Melville, New York) was used to capture the image of the HeNe light emission from the flat fiber [Fig. 2(a)]. Image J (National Institute of the Health, Bethesda, Maryland, USA) was used to measure the HeNe light intensities for quantitative analysis. All the acquired data were filtered to remove low-pass signals and to smooth out the intensity profiles for comparative analysis [26]. The beam radius (or the standard deviation of Gaussian beam) at the surface of the tissue was determined by the position where the optical intensity drops to $1/e^2$ (13.5%) of the maximum intensity.

2.3. Computational analysis

Numerical analysis by using COMSOL Multiphysics software 5.3 (COMSOL Inc., Burlington, MA, USA) was employed to predict temperature development and thermal damage within liver tissue during laser irradiation.

Light distribution

Once an incident laser beam is irradiated onto biological tissue, a portion of the light can be absorbed and scattered within the tissue. Thus, the light intensity in the tissue can exponentially be attenuated along the tissue depth according to the Beer's law as follows [12]:

$$I(r,z,t) = I_0 e^{\left(\frac{-r^2}{2\sigma^2(z)\exp(\mu_s' z)}\right)} e^{(-z(\mu_a+\mu_s'))} \tag{2.1}$$

$$I_0 = \frac{P_{laser}}{\pi s^2} \tag{2.2}$$

where I is the fluence rate along tissue depth z *(W/cm^2)*, I_0 the irradiance at the tissue surface *(W/cm^2)*, μ_a absorption coefficient *(mm^{-1})*, μ_s' reduced scattering coefficient *(mm^{-1})*, $r = \sqrt{\left(x^2 + y^2\right)}$ radial distance *(mm)*, z tissue depth *(mm)*, $\sigma(z)$ the standard deviation of the Gaussian distribution at the tissue depth of z *(mm)*, t time *(sec)*, P_{laser} the modulated laser power *(W)*, and s laser spot radius on the tissue surface *(mm)*.

The first term in the equation *(I_0)* represents the magnitude of incident laser intensity, and the second term illustrates Gaussian distribution of the light intensity on *xy*-plane. The simulated Gaussian beam was spatially diverged from the fiber tip due to NA of the fiber (NA = 0.22) in this study. Thus, standard deviation of the Gaussian distribution at any tissue depth $\sigma(z)$ was calculated in the following manner:

$$\sigma(z) = \sigma(l) + z\tan(\theta_a) \tag{2.3}$$

$$\sigma(l) = \sigma(0) + h\tan(\theta_a) \tag{2.4}$$

where $\sigma(1)$ is the standard deviation of the Gaussian distribution at the tissue interface *(mm)*, $\sigma(0)$ the standard deviation of the Gaussian distribution at the fiber tip [$\sigma(0)$ = fiber radius of 0.2 *mm*], h the distance from the fiber tip to the tissue interface (h = 2.6 *cm*), and θ_a the half acceptance angle of the flat fiber (θ_a = 12.7°). No specular reflection was assumed for the numerical modeling.

Power modulation

During LTC, irradiation time and irradiance are vital to manage the extent of irreversible thermal necrosis within the tissue. Particularly, the constant irradiance to entail the deep coagulation may induce carbonization on the tissue surface due to overheating. In this study, the laser irradiance was, therefore, linearly modulated to attain a pre-determined range of

Biomedical Optics EXPRESS

temperature at the center of the tissue interface. The lower temperature limit was set to be 65 °C (i.e., the threshold of cellular necrosis) while the upper temperature limit was 75 °C (i.e., 10 °C temperature elevation compared with lower limit) [27]. The output modulated power was presented as follows:

$$P_{laser} = mt + P_0 \tag{2.5}$$

where P_0 is the initial power of laser source (W), and m a constant rate of change (i.e., slope of modulated power line). The slope of the modulated power line is a number that illustrates how steeply the line is slanted. In other words, the slope is the ratio between a change in the treatment time (Δt) and the corresponding change in the output power (ΔP_{laser}).

Heat conduction

Theoretically, biological components such as water, chromophores, melanin, and hemoglobin absorb photons from laser light and induce heat to the surrounding tissue [27]. Thermal behaviors in the tissue during the laser irradiation can be expressed by using the Pennes' equation (also called bio-heat transfer equation) as follows [28]:

$$(\rho_{ti} C_{ti}) \frac{\partial T_{ti}}{\partial t} + \nabla(-k_{ti} \nabla T_{ti}) = \rho_b C_b \omega_b (T_b - T) + Q_{met} + Q_{laser} \tag{2.6}$$

where ρ_{ti} is liver tissue density (kg/m^3), C_{ti} specific heat of the tissue ($J/kg{\cdot}K$), k_{ti} heat conductivity of the tissue ($W/m{\cdot}K$), ρ_b blood density (kg/m^3), C_b specific heat of blood ($J/kg{\cdot}K$), ω_b blood perfusion rate (s^{-1}), T_b blood temperature (K), T the local tissue temperature (K), Q_{met} metabolic heat source (W/m^3), and Q_{laser} external heat from laser source (W/m^3). Assuming that both the blood perfusion and the metabolic heat source were considered negligible due to the *ex vivo* conditions, the equation becomes as follows:

$$(\rho_{ti} C_{ti}) \frac{\partial T_{ti}}{\partial t} + \nabla(-k_{ti} \nabla T_{ti}) = Q_{laser} \tag{2.7}$$

$$Q_{laser} = \mu_a I(r, z, t) \tag{2.8}$$

The initial temperature was set to be 20°C, and the external surface of the tissue was considered insulated (i.e., satisfying Neumann boundary condition: $\mathbf{n} \cdot k \cdot \nabla T = 0$ where $\mathbf{n}$ is the normal direction of the heat flux) [28]. The surface radiation was also neglected due to the small temperature difference. The tissue volume was assumed to be large enough for the bio-heat transfer simulation.

Thermal damage

Thermal damage is regarded as an irreversibly denatured process, where native molecules are transformed into a denatured/coagulated state through an activated state, leading to cell death [29]. The extent of thermal damage in tissue could be mathematically illustrated by applying a first-order thermal-chemical rate equation (also called Arrhenius equations). A dimensionless parameter Ω, which depends on the temperature and the exposure time, is used to quantify the degree of thermal damage:

$$\Omega(r,t) = A \int_0^t \exp[-\frac{\Delta E_a}{RT}] dt \tag{2.9}$$

where Ω is dimensionless damage index, A a pre-exponential factor (s^{-1}), ΔE_a activation energy ($J.\ mol^{-1}$), and R the universal gas constant ($J/mol.K$). Both A and ΔE_a are temperature-dependent. Ω = 1 indicates that 63% of tissue experiences the complete cellular necrosis as the temperature rises up to approximately 65 °C [12, 28]. Table 1 summarizes the

Biomedical Optics EXPRESS

optical and thermal parameters of the porcine liver tissue used for the current numerical simulation.

Table 1. Optical and thermal parameters of porcine liver tissues

Parameter	Value	References
Thermal conductivity *k (W/m.K)*	0.513	[19, 30]
Density *ρ* (kg/m^3)	1050	[19, 30]
Specific heat *c (J/kg.K)*	3600	[19, 30]
Absorption coefficient (μ_a, cm^{-1})	19	[30]
Reduced scattering coefficient (μ'_s, cm^{-1})	3	[30]
Frequency factor (A, s^{-1})	5.5×10^{41}	[19, 30]
Activation energy (ΔE_a, *J/mol*)	2.77×10^5	[19, 30]
Universal gas constant (*R, J/mol·K*)	8.314	[19, 30]

2.4. Experimental study

Sample preparation

Porcine liver tissue was harvested from a local slaughter and kept at −15 °C. Each sample was then sliced in a cube of 5 cm × 5 cm × 3 cm (volume = 75 cm^3). All the prepared samples were preserved at 20 °C prior to the experiments.

Laser power modulation

A customized modulator was developed to control laser output power in either constant or linear mode by using pulse with modulation (PWM). A PWM input signal modulates the laser output power by varying the duty cycle of radio frequency (RF) amplifiers from the laser, which in turn controls the time-averaged RF power applied to the laser system. Therefore, a linear power modulation can be created by equally decreasing the PWM duty cycle in each pulse duration. Based upon the preliminary testing, four laser output power conditions were selected and tested for comparison: 2 W constant, 3.5 W constant, 3.5 W slow slope, and 3.5 W fast slope.

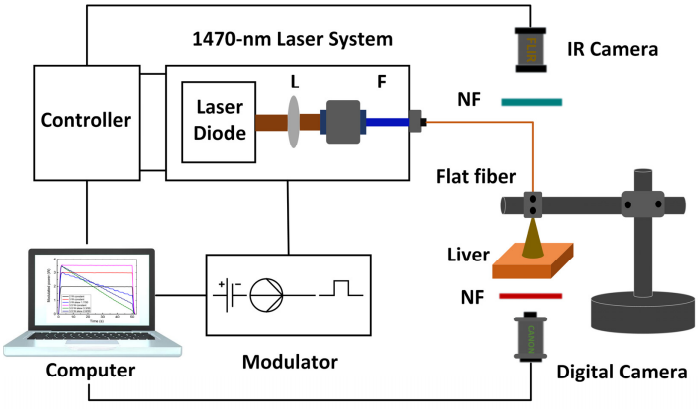

Fig. 1. Experimental set-up for *ex vivo* liver tissue testing (L - lens; F – optical fiber; NF - Neutral filter; IR - infrared).

Experimental set-up

To validate the current simulation model, *ex vivo* experiments were conducted with a flat fiber and liver tissue (N = 5 for each test; Fig. 1). A laser diode system (wavelength = 1470 nm; FC-W-1470, CNI, Changchun, China) was deployed for 50-s laser irradiation. The laser output power was automatically controlled by the customized modulator in four therapeutic

Biomedical Optics EXPRESS

conditions (i.e., 2 W constant, 3.5 W constant, 3.5 W slow slope, and 3.5 W fast slope). During the laser exposure, an IR camera (spectral range of 7.5~13 μm; A325, FLIR, Wilsonville, Oregon, USA) was employed to monitor in real time the temperature increase on the tissue surface, which was used to indirectly assess tissue necrosis. The temporal temperature was measured from the center position of tissue, where the temperature could reach the maximum value. The transient temperature rise was then calculated by dividing the elevated temperature by the corresponding exposure time (i.e., total time to reach maximum temperature). Prior to the IR measurements, liver emissivity was set to be 0.98 to calibrate the camera according to the instructions from the manufacturer's manual [26]. To protect the IR camera from any over-exposure effects, a neutral-density filter was situated in-between the tissue and the camera. The upper surface of the treated tissue was then imaged by using a digital camera (D5100, Nikon Corporation, Tokyo, Japan) with the assistance of a visible neutral filter to evaluate the coagulated tissue area later. Post-experimentally, all the tested samples were stored at −15 °C for an hour and then were cut to photograph the necrosis tissue areas in the cross-sections. The extent of the thermal damage (defined as whitish discoloration) was measured by using ImageJ software for quantitative comparison. Statistical analysis (Student's *t*-test) was performed by using SPSS software (SPSS Inc., Chicago, Illinois), and $p < 0.05$ was considered statistically significant.

3. Results

3.1. Spatial light distribution measurement

Figure 2 explains how to measure the spatial light emission from the flat fiber (digital vs. azimuthal measurement). Overall, the result was in a good agreement with each other, showing the normal Gaussian distribution ("bell shape") with the same standard deviation (σ = 6 mm).

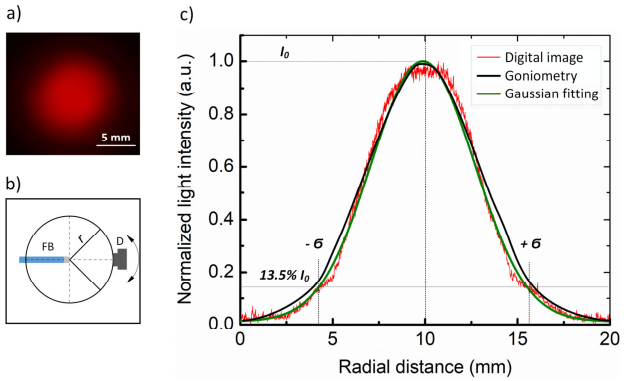

Fig. 2. Normalized spatial light distribution from flat fiber: a) digital image, b) goniometric measurement set-up, and c) light intensity comparison (FB - flat fiber; D – detector; r – rotation radius; I_0 – maximum normalized intensity; σ – beam radius at surface of tissue)

Figure 3(a) illustrates the modulated powers used for the current simulation model while Fig. 3(b) explains the experimental powers which were controlled by the customized modulator. In this study, two power conditions (2 W constant and 3 W constant) were maintained stable throughout the entire period of the treatment, whereas two others were linearly declined with different slopes. The "3.5 W slow slope" condition was generated by setting up the initial power to be 3.5 W, then decreasing it with the slope of 0.056 until it reached to 0.7 W at 50 s. Similarly, the "3.5 W fast slope" condition was created by starting at 3.5 W and reducing to 0.2 W after 50-s power supply time with the faster slant degree of 0.066.

Biomedical Optics EXPRESS

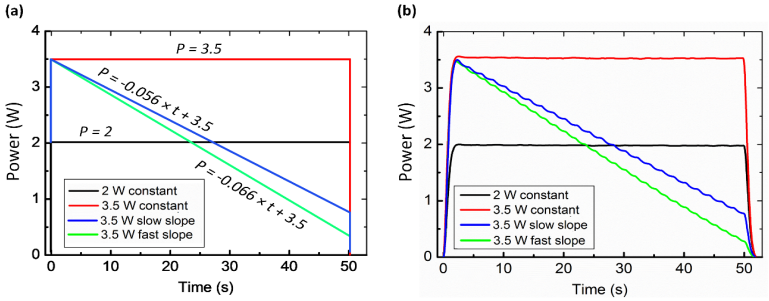

Fig. 3. Power schema under various irradiation conditions (two constant powers and two modulated powers): a) simulation and b) experiment.

Figure 4 represents the temporal development of temperature at the center position of the tissue interface during LTC at various conditions from both simulation and experiment. Overall, the temporal temperatures in Fig. 4(b) show the same tendency as the ones in Fig. 4(a) did. For the simulation case of 2 W and 50 s (Fig. 4(a)), the temperature increased significantly from the initial temperature (20 °C) and reached the peak temperature of 87 °C (transient rise rate = 1.3 °C /s) while the corresponding maximum value was 82.5 °C (transient rise rate = 1.2 °C /s) in the experimental result, which yielded a 4.5-°C difference. Such a trend can be observed with the 3.5-W constant power. The simulated temperature accelerated to the highest maximum of 130 °C (transient rise rate = 2.2 °C /s), which was slightly (7.5 °C) higher than that of the experiments (122.5 °C and transient rise rate = 2.1 °C /s). In contrast to the unmodulated conditions, the modulated powers resulted in more stable temperature outcomes. The simulated "3.5 W slow slope" dose generated the temperature rise to 81 °C after 32-s laser application, and then decreased gradually to 74.6 °C at the end of the treatment. Similarly, the temperature initially developed from 20 °C, reached the peak temperature of 79 °C, and then reduced to 65.7 °C after 50-s treatment in the case of the experimental modulation (blue line in Fig. 4(b)). However, the temperatures almost exceeded the pre-determined range (65~75 °C) in both the simulated and the experimental results. As a consequence, to achieve the expected temperature distribution, the slant degree of the power line should be increased; in other words, laser power should be controlled to be declined rapidly. Apparently, the "3.5 W fast slope" condition represents the longer treatment time within the pre-determined temperature range. In fact, the temperature reached the upper limit (75 °C) and then symmetrically fell off in both the cases, forming a conic with the peak in the middle of the intervals.

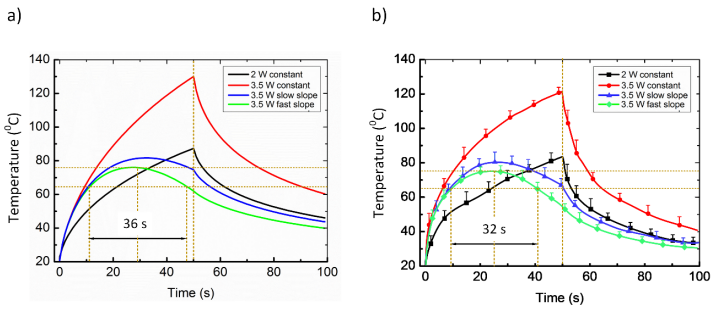

Fig. 4. Temperature development during treatment under various irradiation conditions: a) simulation and b) experiment (N = 5).

Figure 5 depicts the extent of thermal damage at various therapeutic conditions from both simulation and experiment in *xy*- and *yz*-cross sections. Overall, the 3.5-W constant laser power and 50-s irradiation time induced the largest volume of thermal denaturation (i.e., 0.71 cm^3 for simulation vs 0.52 ± 0.10 cm^3 for experiment; approximately 26.7% difference; $p <$

Biomedical Optics EXPRESS

0.01). However, both temperatures were quite higher than the upper limit (75 °C) and thus hardly satisfied the treatment purpose. Figure 5(b) provides the quantitative details of coagulated volumes from the four circumstances (simulation vs experiment). From the simulation, the conditions of "2 W constant" and "3.5 W slow slope" could coagulate the tissue volume of 0.19 cm^3 and 0.28 cm^3, respectively. On the other hand, those values from the experiment were 0.15 ± 0.04 cm^3 and 0.22 ± 0.06 cm^3, respectively ($p < 0.03$). Nevertheless, the temperatures exceeded the pre-determined upper limit (75 °C) during the treatment and seemed unsatisfactory for the treatment goal. Interestingly, the temperatures for the "3.5 W fast slope" could be modulated between the pre-determined lower and upper limits in more than 30 s for both the cases. Moreover, the thermal denaturation volumes were larger than the "2 W constant" situations (0.23 cm^3 vs 0.19 cm^3 for simulation and 0.17 cm^3 vs 0.15 cm^3 for experiment; $p < 0.05$).

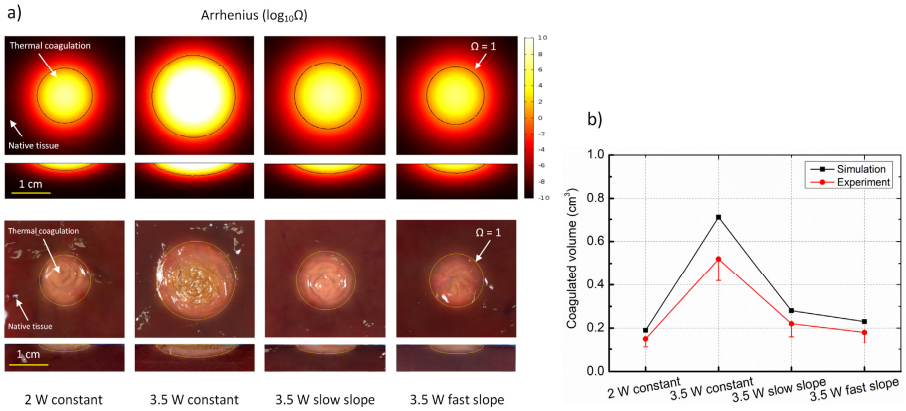

Fig. 5. Thermal damage map under various irradiation conditions: a) corresponding thermal damage with log_{10} of Arrhenius integral (Ω = 1; *top*, and experimental results; *bottom*), and b) coagulated volume from both simulation and experiment (N = 5)

Figure 6 explains how to optimize the therapeutic conditions to induce the pre-determined temperature range between 65 and 75 °C. Before the treatment, many trial tests by changing the initial power and/or the slope were simulated to investigate the optimal condition. Due to the higher transient increase rate of the temperature, the 3.5-W constant power experienced the shorter treatment duration than the 2-W constant circumstance did in both the simulation and the experiment (5 vs. 12 s for simulation and 4 ± 2 vs. 14 ± 3 s for experiment, respectively). However, the surgical time could be extended by linearly modulating the power application. In the simulation results, the "3.5 W slow slope" case could expand the treatment duration up to 9 s which was comparable with the experimental result (15 ± 5 s). Based upon this approach, the "3.5 W fast slope" modulation was numerically investigated as the optimal therapeutic condition along with the coagulated volume of 0.23 cm^3. The current finding was also in good agreement with the experimental outcome (coagulated volume = 0.17 cm^3 and duration time = 32 ± 5 s).

Biomedical Optics EXPRESS

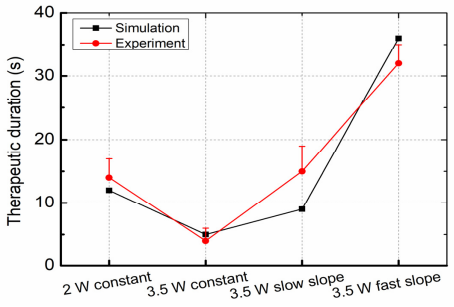

Fig. 6. Comparison of therapeutic durations between simulation and experiment under various conditions (N = 5)

Figure 7 demonstrates the coagulated volume expansions with the time when the temperatures were maintained in the pre-determined range for the "3.5 W fast slope" case. The onset of coagulation (i.e., discoloration) was distinguished by a black line for simulation and a yellow dotted line for experiment. The thermal coagulated effects for both the simulation and the experiment could be visualized after around 10-s irradiation time (coagulated volume = 0.03 cm^3 and 0.02 ± 0.01 cm^3, respectively). After approximately 25-s exposure time, the destructive tissue volumes were extended to be 0.15 cm^3 and 0.11 ± 0.04 cm^3 for the simulated and the experimental results, respectively. Then, the coagulated volume continued to increase up to 0.23 cm^3 (simulation) and 0.17 ± 0.05 cm^3 (experiment) at the end of the treatment.

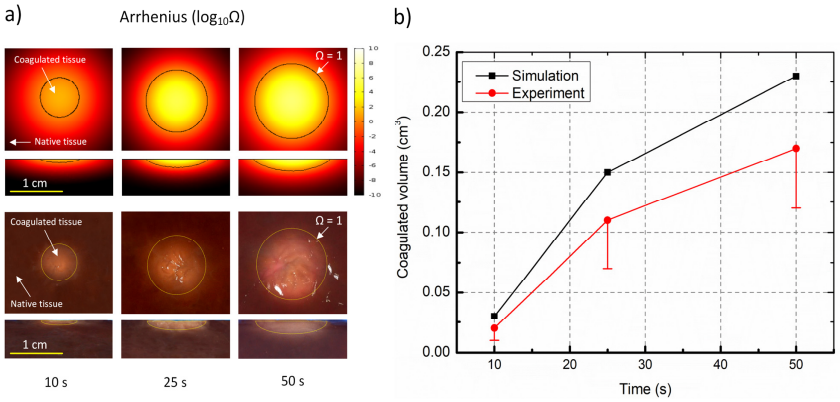

Fig. 7. Thermal damage in ex vivo liver tissue after treatment with 3.5-W fast slope for three different irradiation times: a) corresponding thermal damage with log_{10} of Arrhenius integral (Ω = 1; *top*, and experimental results; *bottom*), and b) coagulated volume from both simulation and experiment (N = 5)

4. Discussion

The main goal of the current simulation model was to evaluate the feasible application of linear energy modulation to predict temperature development and tissue coagulation in a pre-determined manner for effective LTC on small-sized tumors. The pre-determined temperature limits were based upon the threshold for tissue coagulation (lower limit = 65 °C) and upper limit to avoid any carbonization later on (75 °C; 10-°C temperature variation). The end-point of the irreversible thermal destruction was evaluated by solving the Arrhenius equation to find out the boundary between the coagulated and the native tissue regions, where Ω equal to 1 (i.e., temperature for the tissue coagulation threshold) by using COMSOL Multiphysics software. Unlike other commercial software (i.e., ANSYS) that requires laborious coding for mathematical descriptions, the current program was relatively easy to model physical

Biomedical Optics EXPRESS

interplay between laser and tissue due to intrinsic multi-physics modules. However, COMSOL still suffers from extensive memory requirements for solving models with a large number of grid elements, backward compatibility, and difficulty in identifying model inconsistencies [31]. Therefore, in spite of a good agreement between simulation and experiment in the current study, other software should be utilized to validate the proposed model in order to ensure its consistency and accuracy.

Figure 3 showed a slight discrepancy of laser output powers between simulations and experiments (around 2 s at the starting and ending time of laser irradiation). As expected, the laser system should instantly supply the required power for each case. However, continuous wave (CW) 1470-nm diode laser system was modulated by means of the pulse width through the pulse generator (modulator). The time-averaged RF power applied to the laser was controlled by the duty cycle level of the RF amplifier. Therefore, the rising time (transition time) was considered an inherent disadvantage of the CW-laser source. Furthermore, a modest fluctuation in the linear modulation conditions occurred due to large pulse width durations of the modulator (five 10-s intervals in 50 s). Thus, the modulator will be re-designed to decrease the time intervals and to improve the number of pulse width durations, eventually broadening the treatment applications.

The linear energy modulation was fundamentally proposed to maintain almost steady temperature in the pre-determined range with 10-°C fluctuation in this study. The idea was originated from the fact that the customized modulator is only able to modulate the output power in either constant or linear mode. However, with many unexpected variables from tissue (both optical and thermal properties) and laser delivery system (i.e., flat fiber), 10-°C deviation seems too large and less accurate to precisely control the thermal damage in the tissue. On the basis of the current study, other modalities will be implemented to attain the better results once advanced modes (i.e. exponential) are readily available for experimental uses.

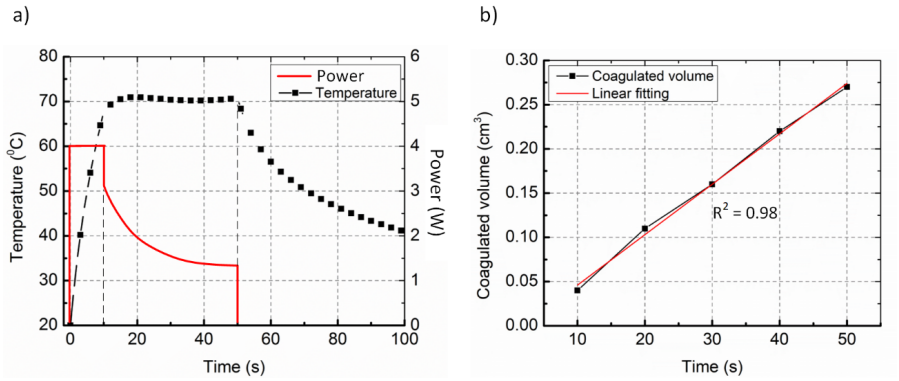

Fig. 8. Temperature development and thermal damage quantification after treatment with combination of CW constant and exponential modes: a) temperature development corresponding to power supply, and b) coagulated volume from simulation

As a dependable demonstration, Fig. 8 illustrates the simulation results of the combined modulation between CW and exponential modes once the expected temperature at the central tissue surface was preset to be 70 °C. 4-W output power was irradiated for 10 s to induce a relative 50-°C increase at the tissue center. It was assumed that if the laser power supply were turned off, the temperature would be declined exponentially to the room temperature. Therefore, in order to indirectly compensate the reduction, an exponential modulation of the output power was employed. It can be seen from Fig. 8(a), the power was instantly decreased to 3.1 W and exponentially dropped out to 1.3 W to invariably maintain the local temperature at 70 °C until the end of the treatment (i.e., 40-s surgical time). Figure 8(b) demonstrates the thermal damage expansion within the porcine live tissue for the corresponding case. After 10-

Biomedical Optics EXPRESS

s treatment with CW 4-W laser, the tissue volume was damaged to be 0.04 cm^3 due to coagulation effects. However, by constantly maintaining the temperature at 70°C for 40 s, the extent of thermal necrosis consistently increased up to 0.27 cm^3 (i.e., seven-fold increase) without any carbonization. As stated in the thermal damage equation, the coagulated tissue volume is primarily a function of the regional temperature and the temporal length of laser irradiation. However, the current method demonstrated that the center point temperature on the tissue surface was steadily maintained at 70 °C; therefore, the magnitude of thermal injury was merely time-dependent. It was also noted that the simulation showed a linear relationship between the exposure time and the necrosis volume (R^2 = 0.98; Fig. 8(b)).

Recently, radiofrequency ablation (RFA), and microwave ablation (MWA) are the most common hyperthermia-based techniques deployed in the clinical application [32, 33]. However, tumors located nearby large blood vessels can be quite difficult to be completely treated by RFA due to heat-sink effect [32]. By contrast, MWA offers advantages including deeper penetration, lager coagulation volume, and less sensitivity to the heat-sink effect, compared with RFA. Therefore, MWA can be beneficial for treating large tumors (> 2-3 cm) such as liver cancer. On the other hand, MWA may be less beneficial for small-sized tumors treatment due to its cumbersome antenna and long treatment time. Thus, LTC with a fine optical fiber and strong light absorption can be an alternative method to readily approach and treat the small-sized tumors (< 2 cm) in a precise and rapid manner [32]. In this model, a 1470-nm wavelength (spot size = 1.2 cm) was selected to facilitate temperature elevation in tissue due to high light absorption [30]. Accordingly, further application of linear energy modulation could avoid superficial carbonization as well as rapidly achieve the pre-determined degree of coagulation in the tissue, which may implicate the feasible treatment of small-sized tumors such as pancreatic adenocarcinoma [33]. Nevertheless, other wavelength lasers should be conducted to investigate the scattering-dominated effects in various tissues and to confirm the versatility of the proposed linear-modulated hyperthermia treatment in terms of temperature development and thermal penetration depth. Regarding IR camera advantages for measuring the temperature development on the tissue surface, the wide temperature area could be controlled instead of only point tracking in order to improve the surgical safety. In addition, as stated in the digital image results, either the fiber fabrication or connection with the laser system was responsible for the unexpected intensity in the center of the spot size (around 10% lower than the Gaussian peak). Moreover, the deployment of a flat fiber was twofold: 1) to simplify geometry of the model and spatial distribution of light for the numerical computation and 2) to incorporate an IR camera to monitor temperature non-invasively during the experiments. In fact, the flat fiber has clinically been used for treating pancreatic adenocarcinoma [33]. However, the flat fiber (i.e., Gaussian beam source) with divergence (NA = 0.22) could induce a high temperature gradient at the tissue center and undesirable errors of thermal damage in the experiments (Fig. 5). Thus, an isotropic fiber (i.e., flat top beam source) in conjunction with an optical collimator should be employed with the proposed technique to achieve uniform thermal damage within the tissue. Furthermore, a radially diffusing optical fiber will be evaluated with the current model to validate its feasible application even for laser interstitial thermotherapy.

Obviously, no thermal confinement took place during laser treatment, in which the laser exposure time exceeded thermal diffusion time (i.e., $t_d = 1/K \cdot \mu_a^2$ = 2 s) [27]. Therefore, light absorption and heat deposition along with thermal diffusion induced the relatively considerable temperature development in the constant power supply mode. The simulated results were attained by using heat conduction equations and sketched out the progressive temperature distribution in the tissue, which was reflected by the experiments apart from the modest inconsistencies. In the case of 3.5 W constant power (Fig. 4), the maximum temperature in the simulation was 6.1% higher than that in the experiment (i.e., 130 vs 122.5 °C). This can be explained by the coagulation effects. Once tissue was thermally damaged, their optical and thermal properties were varied accordingly. As Ritz et al. (2001) suggested

Biomedical Optics EXPRESS

that the scattering coefficient of the completely coagulated tissue increase by seven fold, compared with the fully native tissue [30]. For sake of simplifications, absorption and scattering coefficients were assumed to be invariant in this study. Therefore, the dynamic changes in optical properties of the liver tissue (i.e., absorption and scattering coefficient variations from the completely native tissue to the fully coagulated tissue) should be integrated into the simulated model to further refine the extent of coagulation disruption and to eventually increase the computational accuracy during thermotherapy. Thus, the further investigation will incorporate both temperature-dependent factors of the optical properties and thermal damage index into the current model [19]. Although convective heat loss (i.e., blood perfusion) was insignificant in the current *ex vivo* study, *in vivo* conditions or longer treatment time (several minutes) would need to consider the effect of thermal losses due to heat convection during irradiation. Another explanation of the experimental results could be considered the rising time of the modulator, which may later delay the required powers, compared with the output powers in the simulations.

5. Conclusion

Computational and experimental analysis of thermal response has been performed to investigate the feasibility of linear energy modulation for effective LTC. The temperature was maintained in the pre-determined range to gradually induce thermal coagulative volume within tissue. The proposed modulation technique may be a useful modality to predict temperature distribution and the degree of thermal coagulation in the tissue during LTC.

Funding

Korea Health Technology R&D Project through the Korea Health Industry Development Institute (KHIDI), funded by the Ministry of Health & Welfare, Republic of Korea (grant number: HI16C1017).

Disclosures

The authors declare that there are no conflicts of interest related to this article.